JOURNAL OF GEOPHYSICAL RESEARCH, VOL. 106, NO. A11, PAGES 25,103–25,120, NOVEMBER 1, 2001

Earthward directed CMEs seen in large-scale coronal magnetic field changes, SOHO LASCO coronagraph and solar wind

Yan Li,[1] Janet G. Luhmann,[1] T. Mulligan,[2] J. Todd Hoeksema,[3] C. Nick Arge,[4] S. P. Plunkett,[5] and O. C. St. Cyr[6]

Abstract. One picture of coronal mass ejection (CME) initiation relates these events to the expansion into space of previously closed coronal magnetic fields, often part of the helmet streamer belt. The work described here makes use of the potential field source surface model based on updated synoptic photospheric field maps to study the large-scale coronal field changes. We isolate those field lines that change from closed to open configurations (newly opening field lines) by comparing potential field source surface models from adjacent magnetograph observations, wherein the same starting foot points on the photosphere are used. If there are some newly opening field lines between the times of two maps, we assume there was a possibility for CME occurrence(s) between these times. In particular, if there are newly opening field lines near the solar disk center, an earthward directed CME may have been generated. Monitoring the coronal magnetic field behavior can in principle reinforce (or not) days in advance predictions of magnetic storms based on Solar and Heliospheric Observatory (SOHO) Large-Angle Spectrometric Coronagraph (LASCO) halo CMEs. Moreover, the coronal field over the visible hemisphere contains information about the possible geoeffectiveness of a particular CME because it shows the approximate orientation and location of the active arcades. By comparing halo CMEs with the newly opening field lines, the solar wind measurements from Wind and ACE spacecraft and the *Dst* index, we show that, like soft X-ray sigmoids, disappearing filaments, and Extreme ultraviolet Imaging Telescope (EIT) waves on the disk of the Sun, magnetograph observation-based coronal field models may provide additional information on the likelihood of CME effects at the Earth.

1. Introduction

Coronal mass ejections (CMEs) have attracted much attention in recent years as the link between solar activity, interplanetary disturbances, and geomagnetic storms [*Gosling et al.*, 1991]. Although many recent observations, especially space-based solar observations, provide unprecedented data sets for CME studies and space weather predictions, successful predictions are still a difficult task. Further understanding of the causative solar events is necessary.

Luhmann et al. [1998] initially studied the relationship between CMEs and newly opening large-scale coronal fields due to photospheric magnetic field changes, using potential field source surface (PFSS) models based on magnetograms from Wilcox Solar Observatory (WSO). They found corresponding trends in the temporal behavior of annual averages of inter-Carrington rotation source surface flux increases and the CME rates determined from a variety of observations. This result supports the assumption that CMEs are the primary means by which new solar flux opens to interplanetary space [e.g., *McComas et al.*, 1995] and provides motivation for case studies. While the previous work used photospheric magnetic field Carrington synoptic maps from WSO as the lower boundary condition of the PFSS model for the trend analysis, daily updates of the syn-

[1]Space Sciences Laboratory, University of Calif., Berkeley, California, USA.

[2]Institute of Geophysics and Planetary Physics and Department of Earth and Space Sciences, University of California, Los Angeles, California, USA.

[3]Center for Space Science and Astrophysics, Stanford University, Stanford, California, USA.

[4]Cooperative Institute for Research in Environmental Sciences, University of Colorado and Space Environment Center, and National Oceanic and Atmospheric Administration, Boulder, Colorado, USA.

[5]Universities Space Research Association, Naval Research Laboratory, Greenbelt, Maryland, USA.

[6]Computational Physics, Inc. and The Catholic University of America, NASA-Goddard Space Flight Center, Greenblet, Maryland, USA.

Paper number 2001JA900041.
0148-0227/01/2001JA900041$09.00

optic maps revealed field changes on the timescale of a day that may allow the possibility of visualizing CME sites.

Daily updated synoptic maps are now produced on a regular basis at a few ground observatories in the United States, including WSO (available at http://quake.stanford.edu/~wso/ (1998)), Kitt Peak National Solar Observatory (NSO) (available at http://www.nso.noao.edu/nsokp/nsokp.html (1999)) and Mount Wilson Observatory (MWO) (available at http://www.astro.ucla.edu/~obs/intro.html (1999)). For the case studies in this report we use sequences of daily maps from any of the above three observatories to illustrate comparisons between our modeled newly opening field lines and reported Solar and Heliospheric Observatory (SOHO) Large-Angle Sectrometric Coronagraph (LASCO) halo CMEs [*Plunkett et al.*, 1998; *Webb et al.*, 2000]. Signatures of these CME events in the solar wind (the associated interplanetary CMEs (ICMEs)) are then examined to determine whether the inferred newly opening coronal field arcades provide information on the resulting ICME field orientations as described by *Mulligan et al.* [1998]. Finally by comparing these events with the *Dst* index we show that like Extreme ultraviolet Imaging Telescope (EIT) waves [*Thompson et al.*, 1998], disappearing filaments [*Gosling et al.*, 1974; *Munro et al.*, 1979; *McAllister and Martin*, 2000], and soft X-ray sigmoids [*Canfield* et al., 1999] on the disk of the Sun, magnetograph observation-based coronal field models may provide additional information on the likelihood of CME effects at the Earth.

2. Description of the Coronal Field Analysis

To investigate whether large-scale coronal magnetic fields expand and become open to interplanetary space in response to the photospheric magnetic field changes associated with CMEs, we use the standard potential field source surface (PFSS) coronal model [*Altschuler and Newkirk*, 1969; *Hoeksema*, 1995; *Zhao and Hoeksema*, 1996; *Schatten et al.*, 1969; *Wang and Sheeley*, 1992]. PFSS models use photospheric-magnetic synoptic maps as the inner boundary and a spherical "source surface" (usually at 2.5 R_s) as an outer boundary, where the assumption of radial magnetic field is applied on both boundaries. Laplace's equation for the magnetic potential is solved in the space between the photosphere and the source surface [*Altschuler et al.*, 1977; *Hoeksema*, 1995; *Wang and Sheeley*, 1992], giving a solution represented by spherical harmonics. Using these solutions, we trace the coronal field lines from a fixed grid of starting points on the photosphere to determine the prevailing coronal field configuration. In this paper we use the first nine harmonics to study large-scale field line changes. While not everywhere realistic (currents are known to be present in the corona, especially around active regions), the PFSS model is known for its combination of relative simplicity and ability to approximate coronal hole geometry and eclipse images [*Altschuler et al.*, 1977; *Levine*, 1982; *Gibson et al.*, 1999; *Zhao et al.*, 1999]. In this study we use a spherical source surface position at 2.5 R_s, which has been found by *Hoeksema* [1984] to best replicate interplanetary magnetic field polarities. *Levine* [1982] suggested that a source surface at 1.6 *Rs* was better for solar minimum when comparing predicted open fields with coronal holes, though it is likely that nonspherical source surfaces, described by *Levine et al.* [1982] are more accurate. However, because all PFSS models are still time invariant, nonspherical source surfaces are difficult to apply to realistic solar fields, and the concept of a fixed source surface may be especially compromised during coronal transients, we chose the simplest approach. Our tests showed that 2.5 R_s and 3.25 R_s give very similar field arcades, while 1.6 R_s gives a more structured field line configuration.

To make a daily updated synoptic map used for this study, one merges the latest full disk magnetogram or a central portion of a full disk magnetogram into the left of the previous synoptic map. The latest synoptic map starts from 27 days before until the latest full disk observation. Note that this type of synoptic map differs from the conventional Carrington rotation synoptic map in that it allows the latest magnetic field information to be included and to be used in real time [*Arge and Pizzo*, 2000; J. T. Hoeksema and X. P. Zhao, private communication, 1997]. For further discussions on the different types of synoptic maps in relation with this study, see *Li et al.* [2001].

Field lines are traced for two consecutive updated synoptic maps, starting from the same fixed grid on the photosphere, and are compared. Those field lines that change from closed at the earlier time to open at the next time are isolated and plotted. We refer to these field lines as newly opening field lines. For further description of the method, see *Luhmann et al.* [1998]. If there are significant newly opening magnetic field line arcades between the times of two maps, we assume there is a possibility for CME occurrence(s) between these times. In particular, if there are newly opening field lines near the solar disk center, an earthward directed CME may have occurred.

3. Newly Opening Field Lines and SOHO/LASCO Halo CMEs

Here we present the modeling results on the newly opening field lines for several examples, when SOHO LASCO reported halo or partial halo CMEs. Our aim is to both infer what is happening where coronagraphs give no information behind the occulting disk and compare their geometry as projected beyond the limb. LASCO/C2 or C3 running difference images are used to show a CME snapshot at a particular moment of the transient during the course of its expansion. The images are selected depending on their availabil-

ity, quality, and value in illustrating the transient. The newly opening field lines show where there has been a large-scale reconfiguration of the coronal field involving new expansions into interplanetary space.

The LASCO/C2 imager has a field view of 2 to 6 solar radii, and C3 has a field view of 3.5 to 32 solar radii [*Brueckner et al.*, 1995, data available at http://lasco-www.nrl.navy.mil/about_lasco.html, 2000]. Because it is presumed to image coronal density structures that are confined by coronal magnetic fields, its CME images should bear some resemblance to the involved coronal field geometry. It should be kept in mind when comparing the two that our static potential field models only show what the changing field lines look like before and after a transient reconfiguration, while the LASCO images show the actual transient. Another caveat is that CMEs observed in coronagraph images generally occur on time-scales much shorter than a day (the time interval between the running difference images is approximately 1 hour), and there may have been multiple CMEs during the ~24 hour time period, so that the field changes in our daily updated models likely incorporate more than those occurring in the CME images. The third caveat is that because of the method of construction of the updated synoptic maps we would expect the central disk field to be more accurate than the limb and backside fields, which are based on older photospheric field measurements.

3.1. Example 1

Coronal field lines were traced for the two maps updated on January 5 and 6, 1997, resulting in the newly opening field lines shown in Figures 1a and 1b. Prominent field arcades consisting of well organized, numerous field lines covering the disk were closed on January 5 and open on January 6, at least as seen in the PFSS models. According to our assumption, field lines near the disk center may indicate the occurrence of an earthward directed CME sometime between the observation times of these two magnetograms. The partial halo CME observed at ~ 1600 UT on January 6 by SOHO LASCO is well known for its heliospheric and terrestrial effects [*Webb et al.*, 1998]. It has been reported that this CME was associated with a disappearing filament (DSF) observed between 1301 and 1453 UT and centered at S24 W01. The estimated onset time from LASCO/C2 and C3 is 1402 and 1508 UT, respectively. A LASCO/C2 running difference image at 1734 UT on January 6 is reproduced in Figure 1c (LASCO coronagraph running difference images for halo CMEs are regularly published at the website ftp://ares.nrl.navy.mil/pub/lasco/halo/). As pointed out in the last paragraph, the comparison between the newly opening field lines and the coronagraph difference images is limited by certain factors. The closed and open field line pictures give the before and after states of the changing field lines described by the PFSS model only. The coronagraph images

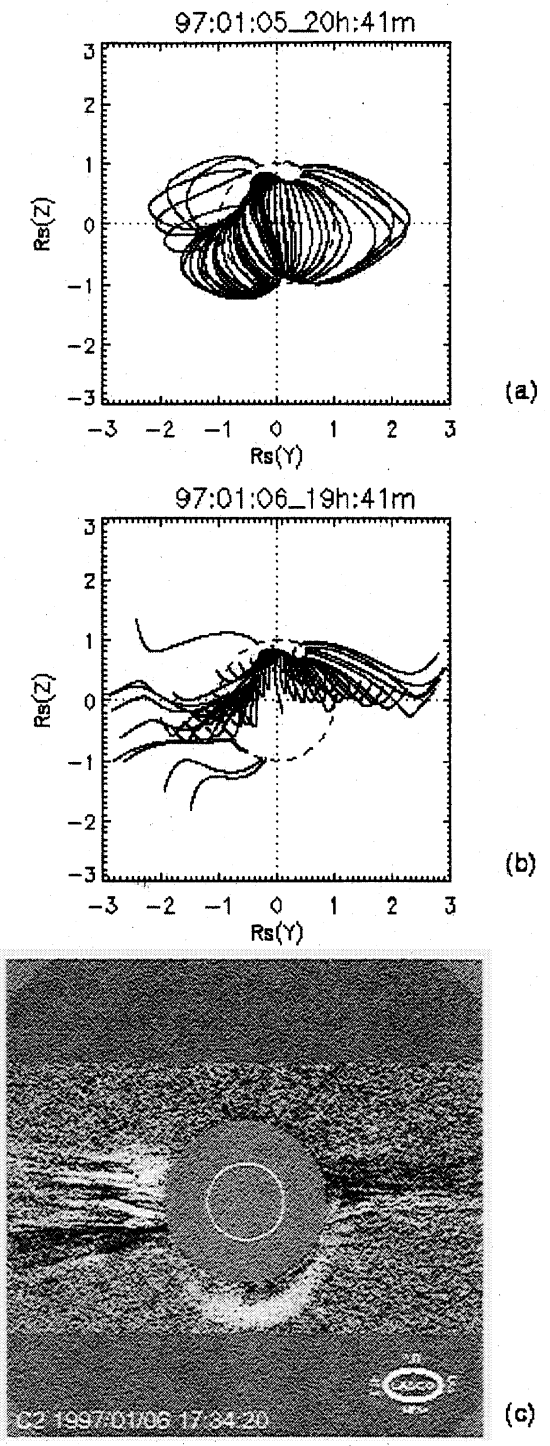

Figure 1. (a and b) Newly opening field lines between January 5 and 6, 1997. These field lines, starting from the same grid points on the photosphere, were all closed on January 5 and all open on January 6. The field line arcade covering the disk center is thought to indicate the occurrence of an earthward directed CME between the observation times. See text for details of the method to isolate newly opening field lines. (c) A LASCO/C2 difference image at 1734:20 UT, January, 1997.

are snapshots of the CME expansion process in between these two states. The difference images bring out projected locations where the density is changing between snapshots. In this case, the coronagraph dif-

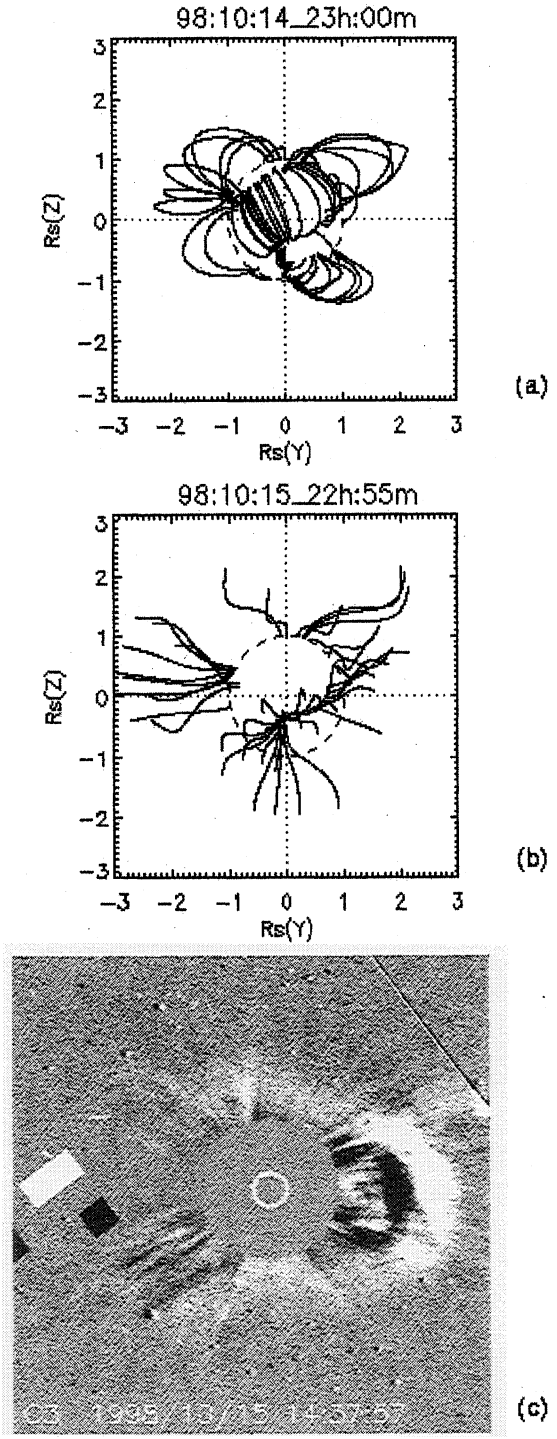

Figure 2. (a and b) Newly opening field lines between October 14 and 15, 1998. The group of field lines covering the disk center is thought to indicate the occurrence of an earthward directed CME between the observation times. (c) A LASCO/C3 difference image at ~ 1437:57 UT, October 10, 1998.

ference image in Figure 1c shows density changes along the east and west streamer belt and a partial halo at the south. We also see some newly opening field lines at the limbs around the east and west streamer belts and toward the Earth from Figure 1a and 1b. Further images and movies of this CME may be found at ftp://ares.nrl.navy.mil/pub/lasco/halo/.

3.2. Example 2

Coronal field lines were traced for the two maps updated on October 14 and 15, 1998, resulting in the newly opening field lines shown in Figures 2a and 2b.

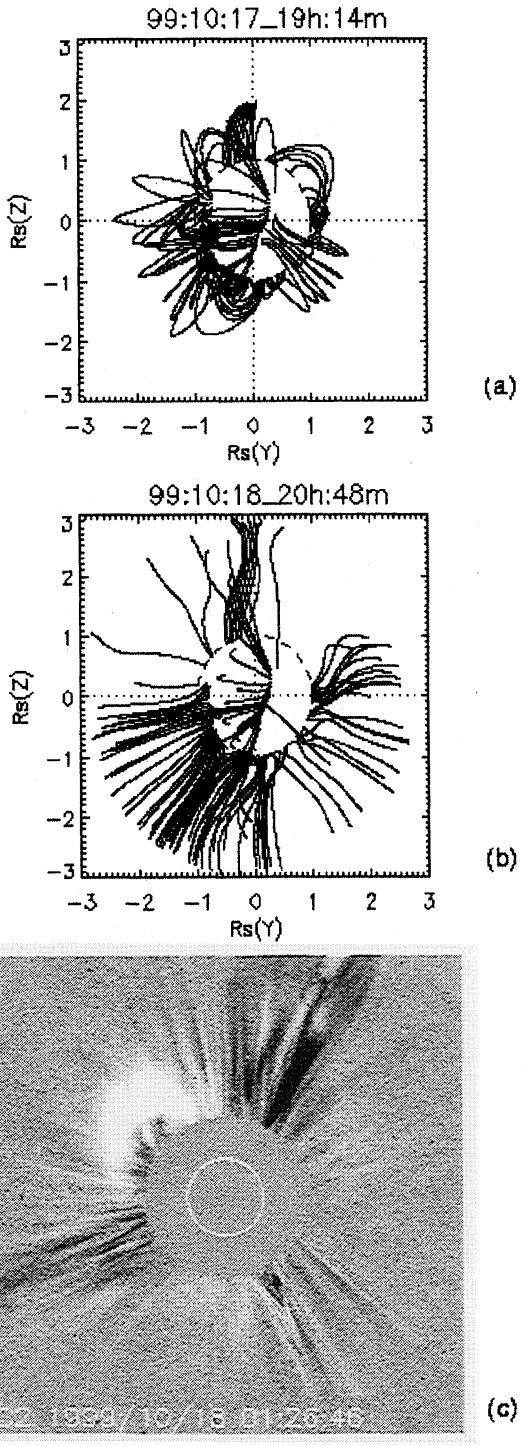

Figure 3. (a and b) Newly opening field lines between October 17 and 18, 1999. An earthward directed CME between the observation times is expected. (c) A LASCO/C2 image at 0126:46 UT, October 18, 1999.

Well-organized field arcades covering most of the disk from the southeast limb across the disk center to the northwest limb were closed on October 14 and open on October 15. There was a LASCO halo CME on October 15 at ~ 1004 UT, reported as a bright symmetrical halo with a filament eruption and two ribbon flare in EIT observations (available at http://lasco-www.nrl.navy.mil/cmelist.html (2000)). A LASCO/C3 running difference image is reproduced in Figure 2c at 1438 UT on October 15, which shows a halo around the disk and a rapidly changing expanding loop in progress at the west limb. The significant newly opening field arcades directed toward the Earth are consistent with the halo CME. But a prominent opening loop at the northwest corner slightly <45° from the equator appears to be at a somewhat different location from the expanding loop at the west limb seen in the coronagraph difference image. It is interesting to note that the disappearing filament on this day was located at the northeast (NSO Hel10830, SOHO/EIT, and Yokoh SXT images are available at http://sprg.ssl.berkeley.edu/mf_evol/), but the feature that looked like a prominence inside of a bright loop CME (e.g., a light bulb event) was at the west limb. However, it is not uncommon to find EIT events lying well away from the apparent central axis of the CME in LASCO.

3.3. Example 3

Newly opening field lines between October 17 and 18, 1999, are shown in Figures 3a and 3b. Again, field arcades consisting of well-organized field lines cover the center left part of the disk from the north across to the south. An earthward directed CME is thus expected to take place between the October 17 and 18. LASCO reported that at the beginning of October 18 (0006 UT) a loop-like leading edge, with a faint extension over the south pole, may be forming a partial halo. The LASCO/C2 difference image in Figure 3c at 0127 UT on the October 18 shows an expanding loop at the northeast corner and apparent density changes along the three streamers. In late 1999 the Sun is more active, and the magnetic fields are more complex. Direct comparison between the field line changes over the time of one day and the coronagraph snapshots is expected to be more difficult. At least in this case, the expanding loop at the northeast corner in the C2 image may represent the process of the opening up of the modeled field line loops at the approximately same location.

3.4. Example 4

Newly opening field lines between June 1 and 2, 1999, are shown in Figures 4a and 4b. In this example there are many newly opening field lines around the limb and the poles, but only a few are scattered on the disk center. This picture indicates that there should not be a significant earthward directed CME during these 2 days. However, LASCO reported a bright structured halo at

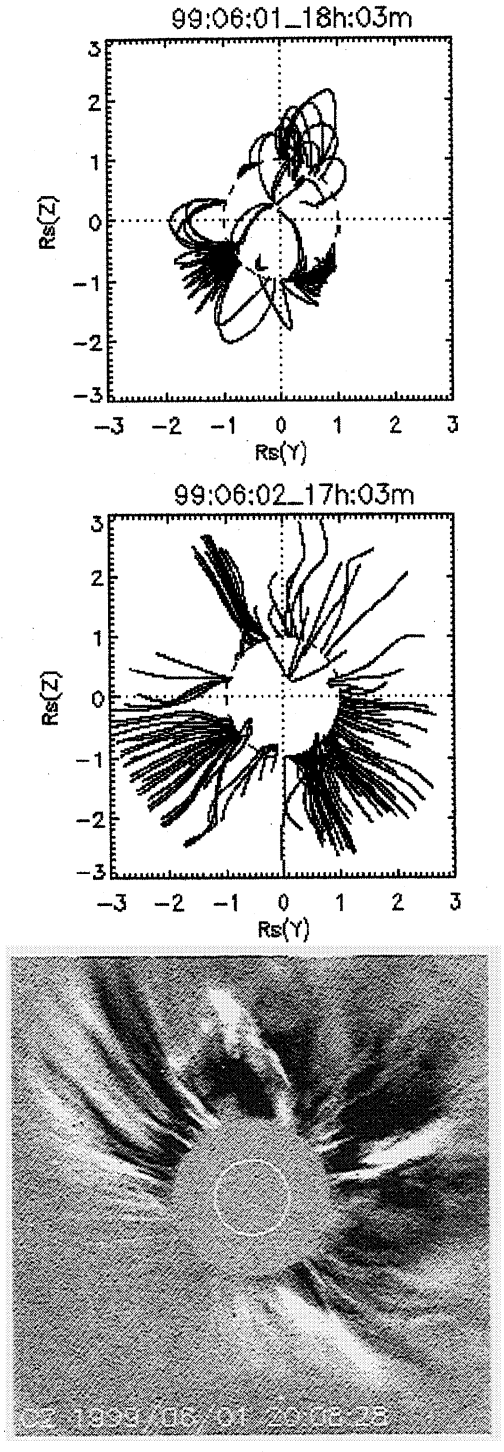

Figure 4. (a and b) Newly opening field lines between June 1 and 2, 1999. There are no newly opening field lines near the disk center in this case. Therefore no earthward directed CME is expected between the observation times. (c) A LASCO/C2 difference image at ~ 2008:28 UT, June 1, 1999.

1937 UT, June 1. A LASCO/C2 difference image is shown in Figure 4c at 2008 UT on the June 1, which shows an expanding loop at the North Pole and density changes around the disk. This was a rapidly changing event in the more active period in mid-1999. Detailed

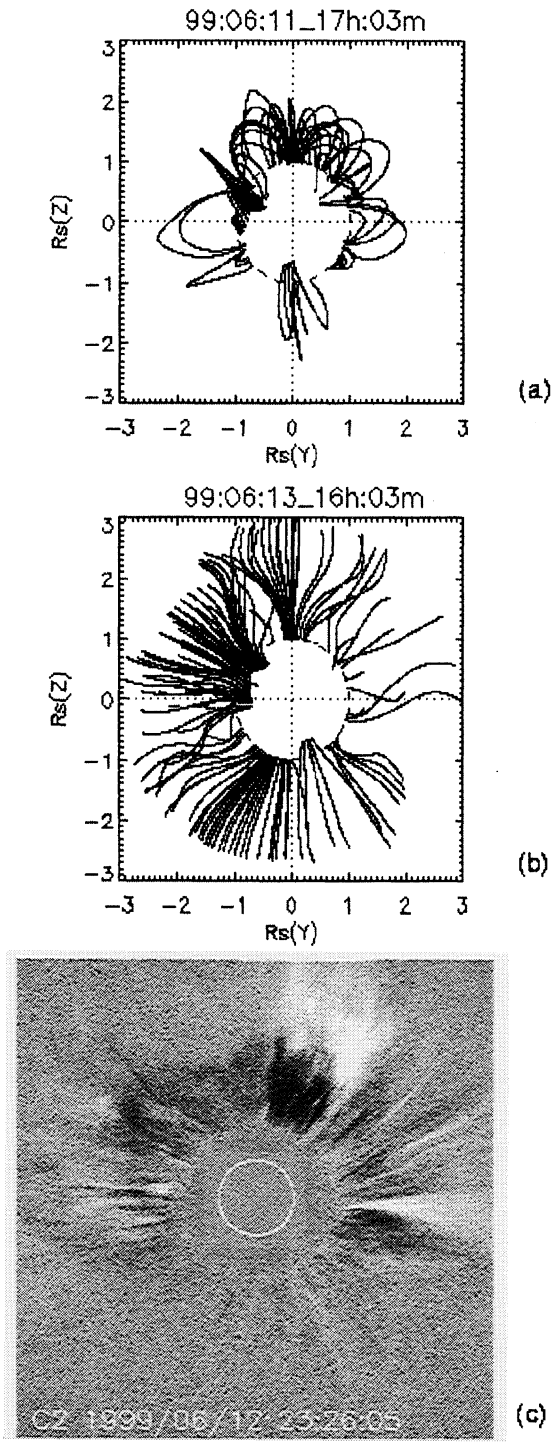

Figure 5. (a and b) Newly opening field lines between June 11 and 13, 1999. No earthward directed CME is expected between the observation times. (c) A LASCO/C2 difference image at ~ 2326:05 UT, June 12, 1999.

comparison between the 1-day field line changes and the ~1 hour difference image of the coronagraph snapshots is again ambiguous. The expanding loop at the North Pole in the C2 image may represent the opening up of the modeled field line loops near the North Pole.

3.5. Example 5

Newly opening field lines between June 11 and 13, 1999, are shown in Figures 5a and 5b. There was no magnetograph observation on June 12. There are some opening field lines around the limb and poles but no field lines near the disk center. We thus expect no earthward directed CME during these days. However, as in the previous case, LASCO reported a halo CME. The halo CME occurred around 2126 UT on June 12, and possibly consisted of multiple events. A LASCO/C2 running difference image is shown in Figure 5c at 1223 UT on June 12. The field line changes modeled for this event are over 2 days. Only some features at the northwest corner and the east limb arguably correspond in the modeled field lines and the C2 image.

3.6. Example 6

Newly opening field lines between June 23 and 24, 1999, are shown in Figures 6a and 6b. Again some newly opening field lines occur around the limb but none near the disk center. LASCO reported a partial halo CME around 1331 UT with a filament eruption on June 24. A LASCO/C2 difference image is reproduced in Figure 6c at 1430 UT on June 24, which shows a faint expanding loop at the northwest corner and ray structures almost evenly distributed around the disk except for the south polar region. The opening field line loops above the diagonal line connecting the northeast and southwest corner in the two field line pictures seem to correspond to the expanding loop feature and the line structure in the C2 image. Below that diagonal line there are almost no changing field lines except for the dense group in a small area near the South Pole that is not seen in the C2 image. Again, we do not expect them to show the same features given the level of solar activity and our approximations.

While these comparisons are qualitative, overall they show occasional agreements with some features despite the approximations made in the PFSS models. Also, it is unclear exactly what the LASCO difference images show in relation to coronal field lines at the time of the transient (e.g., there may be contributions to the LASCO-imaged electron densities from compressed regions in front of ejecta). Nevertheless, the value of the latter is in their potential ability to give information on the fields leaving the Sun with the CME, or on the ejection of an Earthbound transient.

While our aim here is to study the relationship between near-disk-center newly opening field lines and halo CMEs, it is also interesting to consider whether the newly opening field lines on the solar limb agree with LASCO CME limb events occurring in the interval used for the field line calculations. There was only one halo CME between each pair of magnetograms in the six examples above. Apart from the halo CME, there was one limb CME reported between the two magnetograms on January 5 and 6, 1997; four limb CMEs

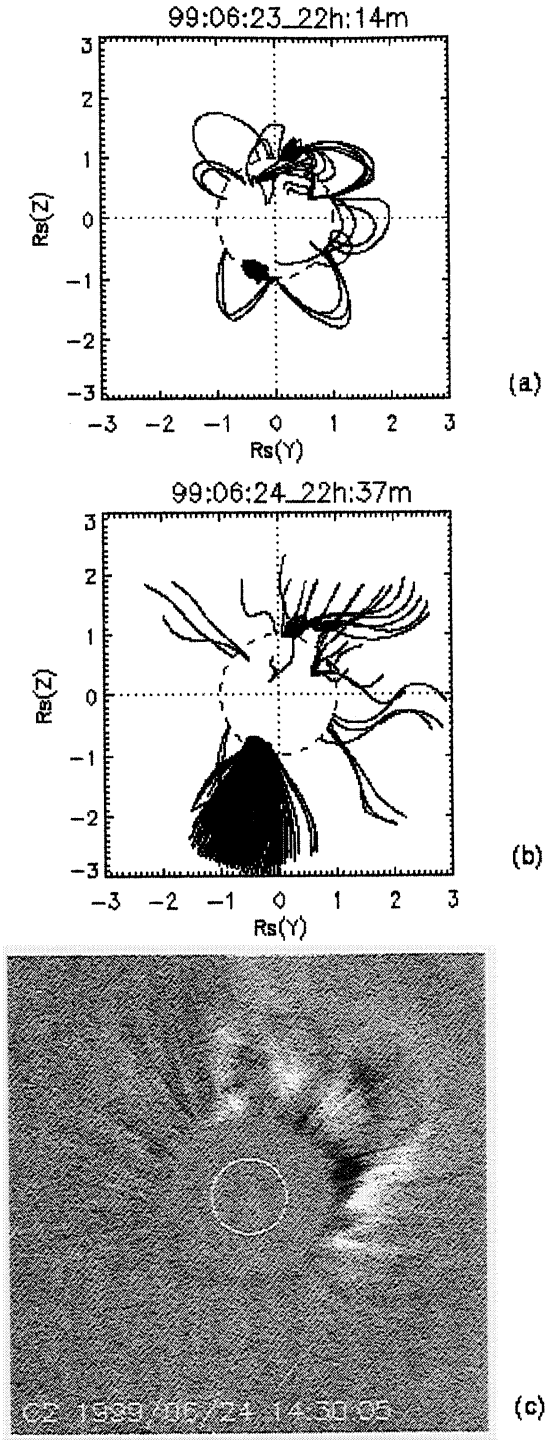

Figure 6. (a and b) Newly opening field lines between June 23 and 24, 1999. No earthward directed CME is expected between the observation times. (c) A LASCO/C2 difference image at ~ 1430:05 UT, June 24, 1999.

were reported between the two magnetograms on October 17 and 18, 1999; four limb CMEs were reported between the two magnetograms on June 1 and 2, 1999; five limb CMEs were reported between the two magnetograms on June 11 and 13, 1999; and two limb CMEs were reported between the two magnetograms on June 23 and 24, 1999. For the October 14 and 15, 1998 case, SOHO was not in operation until the October 15, so we do not have a complete record. We will not describe these limb CMEs in detail but only point out the following. Figures 1b and 6b suggest fewer newly opening field lines around the limb, while Figures 3b, 4b, and 5b show a more substantial number of newly opening field lines around the limb. Thus it appears that for more CMEs, more newly opening field lines were indicated by the PFSS models. The limb is not where the best comparison is expected between the model results and the observations because of the way the synoptic maps are constructed (older data to the east and west of the central meridian of the latest magnetogram) and the intrinsic problem of the polar field observations. To apply this approach to the global Sun, one would have to have accurate information for all solar longitudes.

4. Modeling the Flux Rope Structure of Interplanetary Coronal Mass Ejections

Mulligan and Russell [2001] applied a divergence free magnetic flux rope model using exponential distributions for magnetic field strengths to infer the size, orientation, and field strength of observed interplanetary magnetic clouds [*Burlaga*, 1988; *Lepping et al.*, 1990]. The model can create both cylindrically symmetric and oblate magnetic topologies, and the former is used for this paper. The model uses 10 parameters to describe the cylindrically symmetric flux rope, i.e., two field strengths (the maxima of the poloidal and axial field strengths), two exponential widths, two exponential powers, two angles (clock angle and cone angle, explained below) that determine the orientation of the symmetry axis, an impact parameter (the distance of the closest point of observation to the flux rope axis), and an expansion factor that aids in determining the degree of asymmetry between the leading edge and trailing edge of the rope. In solar-equatorial coordinates (X axis, towards the Sun along the Earth-Sun line, Y axis, eastward; and Z axis, solar north) the clock angle is defined in the Y-Z plane in a counterclockwise sense with 0° corresponding to the axial field along the Z axis. The cone angle is defined such that it is 0° when the axis of the rope is aligned along the X axis. For detailed descriptions of the model see *Mulligan and Russell* [2001].

5. Signatures in the Solar Wind

The ACE spacecraft at the L1 point has been making measurements of the solar wind parameters upsteam of the Earth on a regular basis since 1998 [*McComas et al.*, 1998; *Smith et al.*, 1998]. Also, the Wind spacecraft with an Earth orbit has been making measurements of the solar wind parameters since late 1994 [*Lepping et al.*, 1995; *Ogilvie et al.*, 1995]. Here we use the ACE plasma data from the solar wind electron pro-

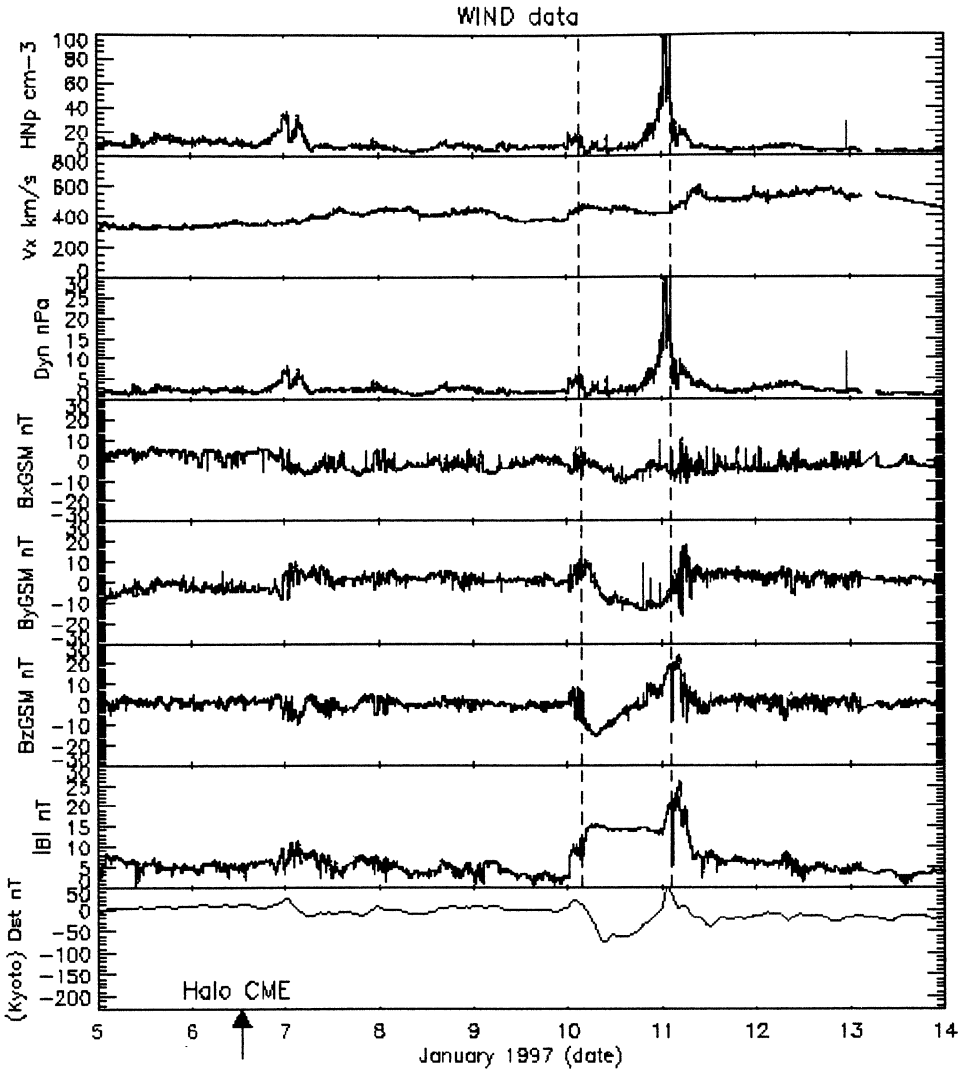

Figure 7. Solar wind parameters from Wind spacecraft for January 5 to 13, 1997. The proton density, solar wind speed and dynamic pressure from the Solar Wind Experiment (SWE) are reproduced in the upper three panels, the magnetic B_y, B_z and B total from Magnetic Fields Investigation (MFI) are in the next three panels, and the bottom panel contains Kyoto *Dst* measurements.

ton alpha monitor instrument [*McComas et al.*, 1998] and the ACE magnetic field measurements from the MAG magnetometer [*Smith et al.*, 1998]; from Wind we use the Solar Wind Experiment plasma data [*Ogilvie et al.*, 1995] and MFI magnetic field data [*Lepping et al.*, 1995]. We search for the interplanetary counterparts of the previously described CMEs (the ICMEs) in Wind or ACE solar wind data (e.g., using data available at http://www-ssc.igpp.ucla.edu/forms/polar/corr_data.html (2000)).

The solar wind proton density, speed, and dynamic pressure are reproduced in the upper four rows in Figures 7, 10, 13, 16, 17, and 18, the magnetic field components B_x, B_y, B_z and B total are in the next four rows, and the bottom row contains the Kyoto *Dst* index. The solar wind data in Figure 7 that cover January 5 to 14, 1997, are from Wind. The abscissa is the day of the month, and each date marks the beginning of the day. The arrow marks the time of occurrence of the halo CME on January 6 described in example 1 (section 3.1). An ICME is seen starting at the beginning of January 10 ~82 hours after the halo CME and continuing until early on January 11, characterized by a slight increase and oscillation in the proton density and coherent rotations in the magnetic field components. The implied average Sun-to-Earth speed of the CME based on the time of arrival at 1 AU is ~507 km/s. During the ICME the B_y component rotated gradually to a westward field and reached -17 nT, and the B_z component rotated quickly to a southward field, reached -20 nT, and rotated gradually back to northward. The southward B_z lasted for ~12 hours. The solar wind speed at 1 AU has a slight increase and remained moderate at ~400 km/s during the ICME.

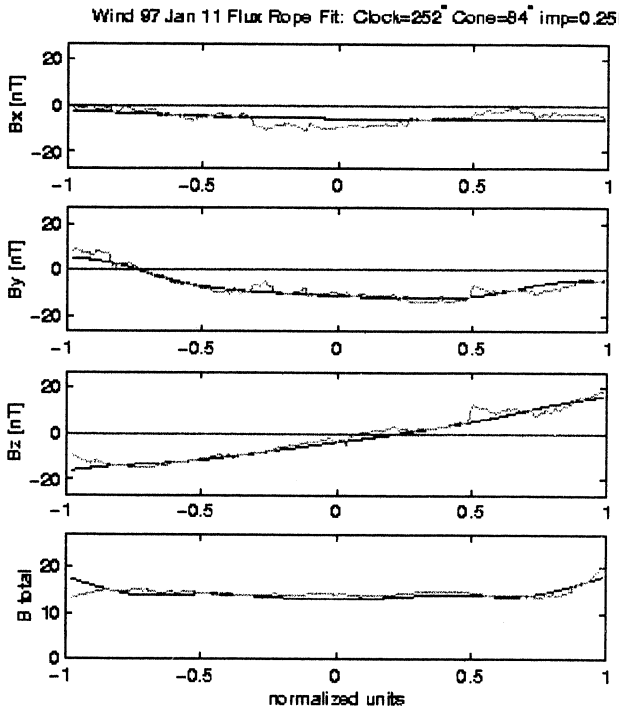

Figure 8. Magnetic field components of the flux rope model (see text for details) overlapped on the Wind magnetic field data between the two vertical dashed lines in Figure 7 for the January 10, 1997 ICME, where the smooth dark lines are the model and the lighter lines are Wind magnetic field data.

Assuming the ICME magnetic field signatures are given by a flux rope configuration [*Mulligan et al.*, 1998; *Mulligan and Russell*, 2001; *Lepping et al.*, 1990], we fit the data to a flux rope model using the interval between the dashed vertical lines in Figure 7. The fitting is shown in Figure 8, where the smooth dark lines are the model and the lighter lines are Wind magnetic field data between the two vertical dashed lines in Figure 7. A three-dimensional (3-D) cylinder plot of the outer boundary of the fitted flux rope model as viewed from the Earth is shown in Figure 9. The flux rope axis has a clock angle of 252°. If we consider that the field line arcades in Figure 1a form the outer part of the flux rope observed at 1AU [e.g., *Gosling*, 1990], the axis of the field line arcades at the disk center makes a similar clock angle when compared with the fitted model of the ICME. It should be noted that we do not expect these axes to match precisely because of the distortions of ICMEs in transit from the Sun by solar wind stream structure [e.g., *Odstrcil and Pizzo*, 1999] and the approximations in both the PFSS model and the flux rope model.

The ACE measurements and Kyoto *Dst* plot are reproduced in Figure 10 covering October 14 to 22, 1998. The arrow marks the time of occurrence of the halo CME on October 15 described in example 2 (section 3.2). An ICME is seen starting late on October 18 ~84 hours after the halo CME and continuing on through October 19, characterized by an increase in the proton density and sudden changes in the magnetic field. The implied average Sun-to-Earth speed of the CME is ~495 km/s. During the ICME the B_y component shows a westward field that reached -20 nT, and the B_z component shows a southward field that reached -20 nT, remaining fairly constant for ~10 hours. The solar wind speed at 1 AU has a slight increase and remained moderate at ~400 km/s during the ICME.

The flux rope fit for this case was done using the magnetic field data between the dashed vertical lines in Figure 10. The fit is shown in Figure 11, where the smooth dark lines are the model, and the lighter lines are the ACE magnetic field data between the two vertical dashed lines in Figure 10. The 3-D cylinder plot as viewed from the Earth for this case is shown in Figure 12. The flux rope axis has a clock angle of 141°. The axis of the field line arcades in Figure 2a again has a

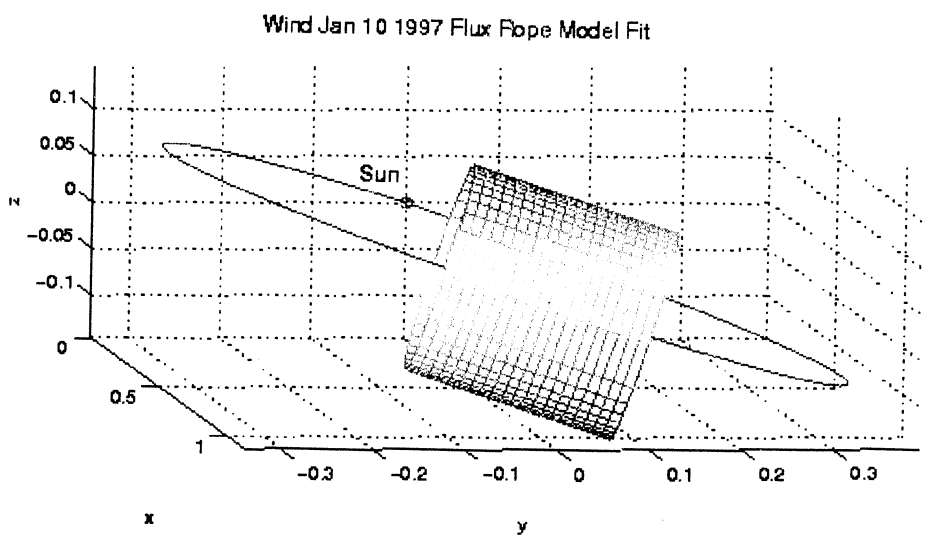

Figure 9. A 3-D cylinder of the modeled flux rope for the January 10, 1997 ICME, viewed from the Earth. The orientation agrees quite well with the newly opening field arcade in Figure 1a.

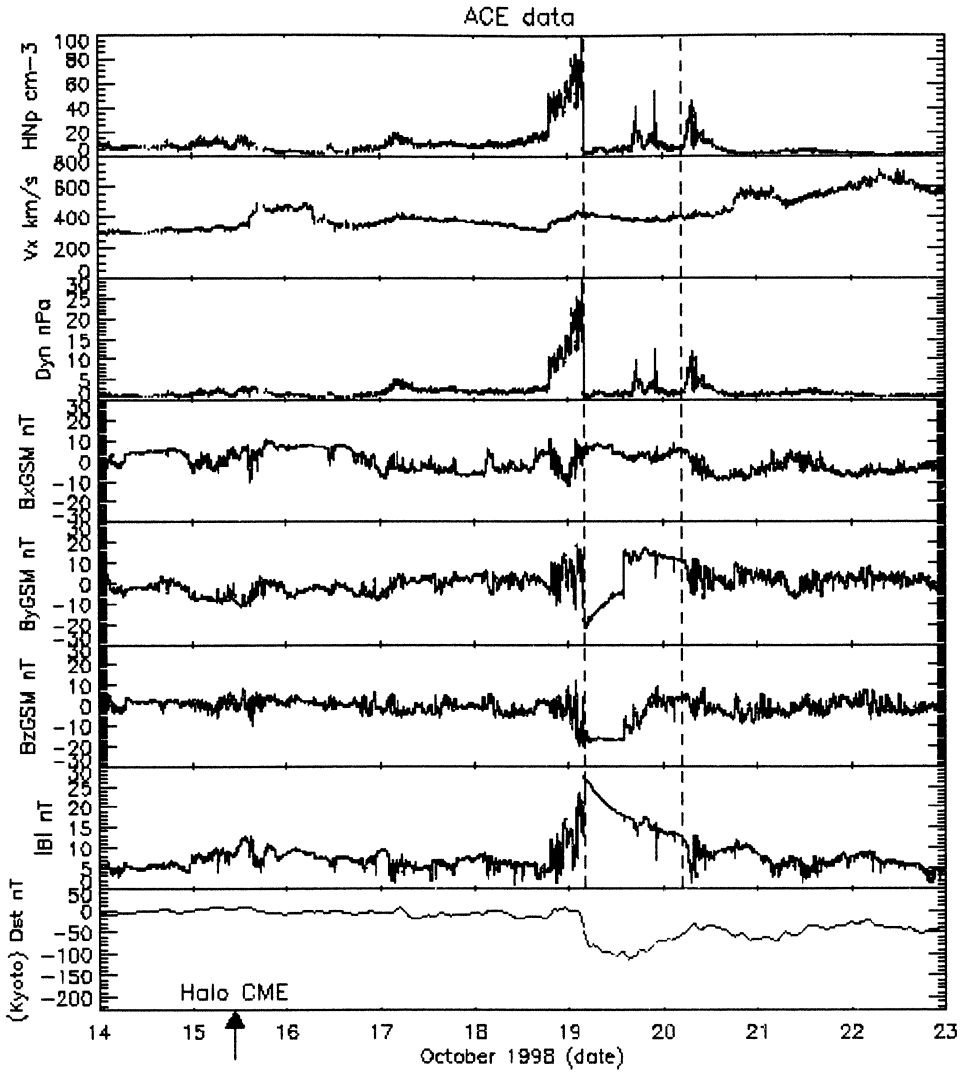

Figure 10. Solar wind parameters from Ace spacecraft at L1 point for October 14 to 22, 1998. The proton density, solar wind speed, and dynamic pressure from the SWEPAM instrument are reproduced in the upper three panels, the magnetic B_y, B_z and B total from the MAG instrument are in the next three panels, and the bottom panel contains Kyoto *Dst* measurements.

somewhat smaller clock angle than the fitted model of the ICME, but the orientation is in basic agreement. Note that the magnetic field discontinuity (seen in the B_y component in the fifth panel of Figure 10) may raise concern as to whether it is valid to assume a fluxrope configuration for this ICME. The plasma data indicated no apparent discontinuity in speed (second panel of Figure 10) or in the proton temperature (it remained cold; not shown here). The speed is smoothly decreasing, which is typical of classically expanding magnetic clouds (as the declining B total field profile suggests). A few density enhancements exist in the latter part of the cloud, but the density signature within a magnetic cloud is often variable. Also, it is not uncommon to see flux ropes with "kinks" that locally distort the flux rope structure.

The same ACE measurements and Kyoto *Dst* plot are reproduced for October 17 to 25, 1999, in Figure 13. Disturbances in the solar wind began 72 hours after the halo CME on October 18 with a large increase in density and not much change in speed, with an abrupt eastward increase of B_y, and a gradual north turning of B_z. The implied average Sun-to-Earth speed of this CME is ~577 km/s. After the initial disturbances the density changed back to a low level for over a day, B_y stayed eastward for slightly under a day, and B_z slowly rotated north and back in the meantime. This sequence of events is followed by an oscillation in density, with B_y rapidly turning west and B_z sharply turning south to reach a minimum of -30 nT, and remaining southward for ~6 - 7 hours.

The magnetic field signatures of this ICME are not well characterized by the classical flux rope picture. Nevertheless, we also carried out a flux rope model fitting for this case, using the magnetic field data between the two dashed vertical lines in Figure 13. The resulting

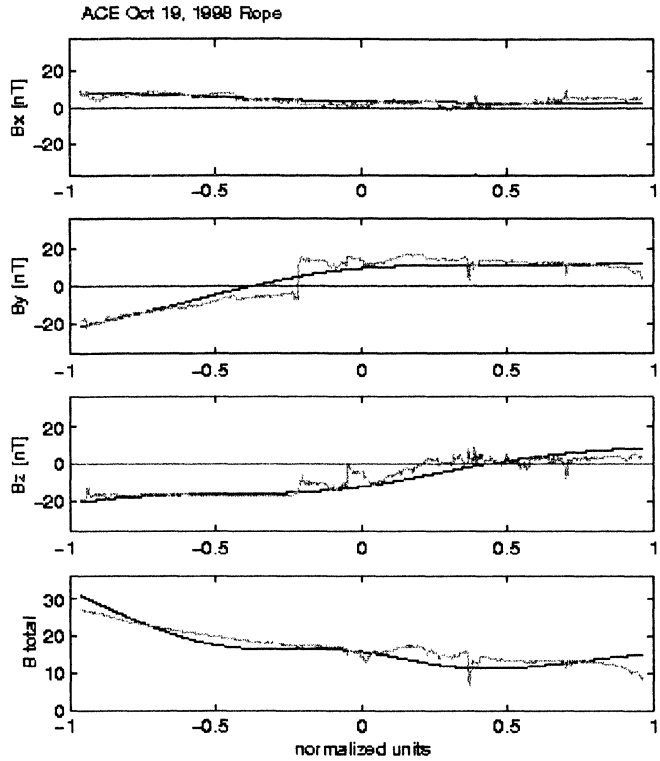

Figure 11. The magnetic field components of the flux rope model overlapped on the ACE magnetic field data between the two vertical dashed lines in Figure 10 for the October 19, 1998 ICME, where the smooth dark lines are the model and the lighter lines are Wind magnetic field data.

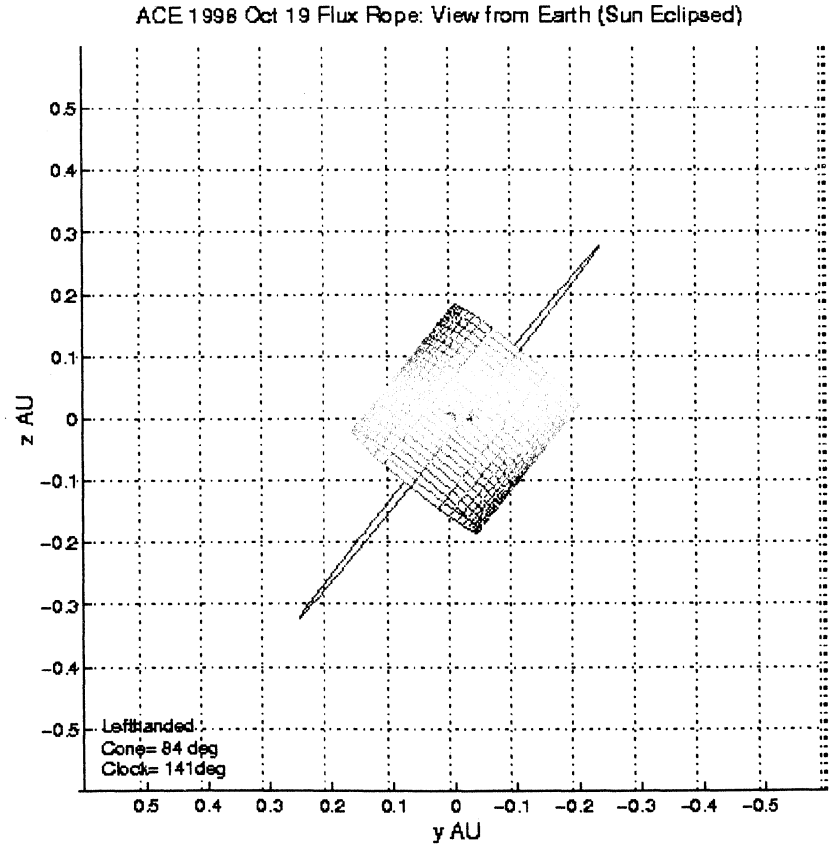

Figure 12. A 3-D cylinder of the modeled flux rope for the October 19, 1998 ICME, viewed from the Earth. The orientation agrees quite well with the newly opening field arcade in Figure 2a.

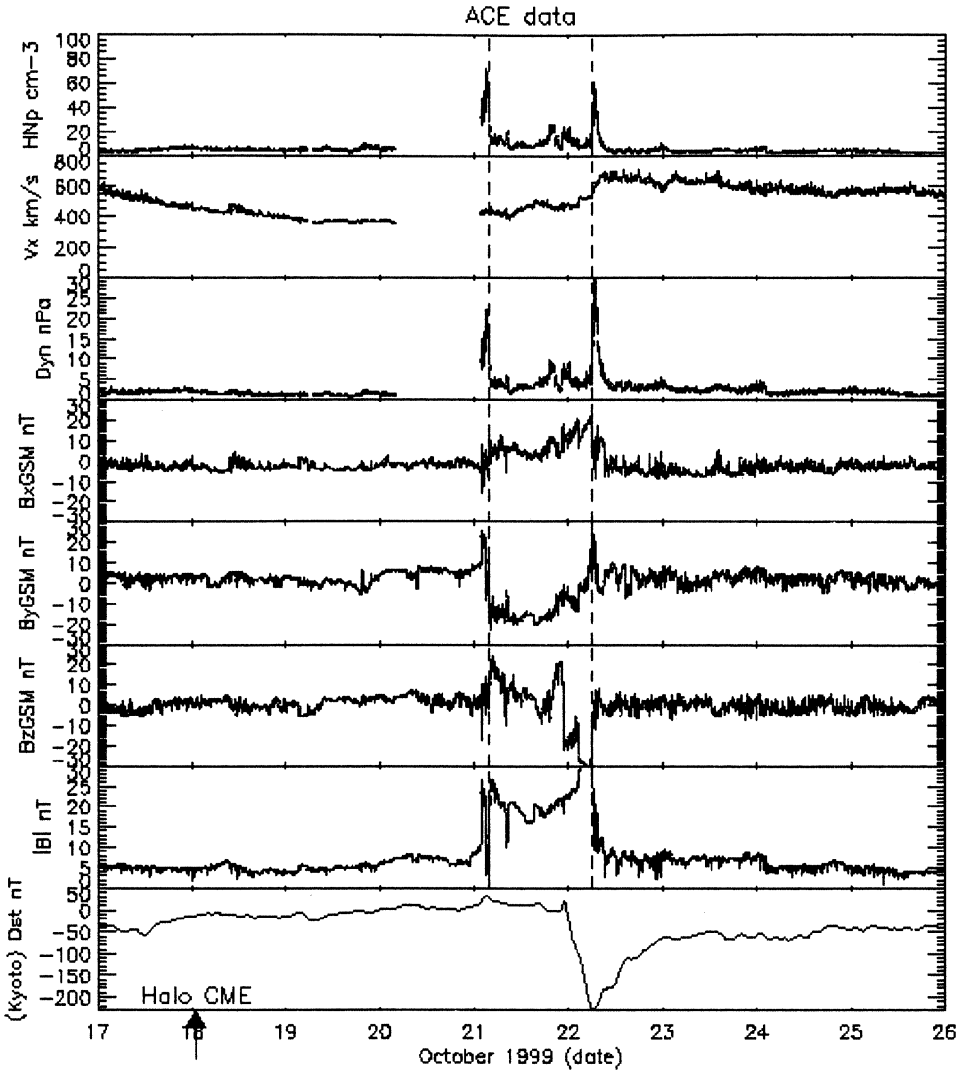

Figure 13. Same as in Figure 10, but for October 17 to 25, 1999, from ACE.

fit is shown in Figure 14, where, as before, the smooth dark lines are the model, and the lighter lines are ACE data between the two vertical dashed lines in Figure 13. The 3-D cylinder plot as viewed from the Earth is shown in Figure 15. This flux rope axis has a clock angle of 261°. The newly opening field arcades for the CME in Figure 3a have a north-south orientation, which is almost perpendicular with the axis of the fitted flux rope. From the newly opening field line highly inclined field arcades we expect a unipolar magnetic field signature in the ICME (southward in this case). The observed magnetic signature is instead rather complex, which might be expected considering it occurred in late 1999 when solar activity is approaching its maximum and the solar magnetic fields become more complex than for the two previous cases in 1997 and 1998. In a paper by *Mulligan et al.* [1998] a study of the variation of the flux rope orientation with solar activity cycle has shown that highly inclined ropes are common during solar maximum. It is also likely that the simple flux rope geometry that fits less than ~30% of ICMEs overall [e.g., *Gosling et al.*, 1990] more often fails at solar maximum. This hypothesis is, unfortunately, difficult to test because of the problem in even distinguishing ICMEs in the solar wind around solar maximum.

The same ACE measurements and Kyoto *Dst* plot are reproduced for June 1 to 9, 1999, in Figure 16. There is clearly no ICME signature during this period, despite the halo CME late on June 1 described in example 4 (section 3.4). The June 12 to 20, 1999, ACE data in Figure 17 show some small oscillations in both the magnetic field and solar wind parameters beginning ~30 hours after the halo CME late on June 12 (example 5; section 3.5), but considering that the ICME speed remained below 400 km/s, we consider the disturbances at 1 AU unrelated to the CME which should arrive more than 2 days later. No other ICME signature was seen in the following days shown in the plots. The ACE measurements for June 22 to 30, 1999, are plotted in Figure 18. Small disturbances starting early on

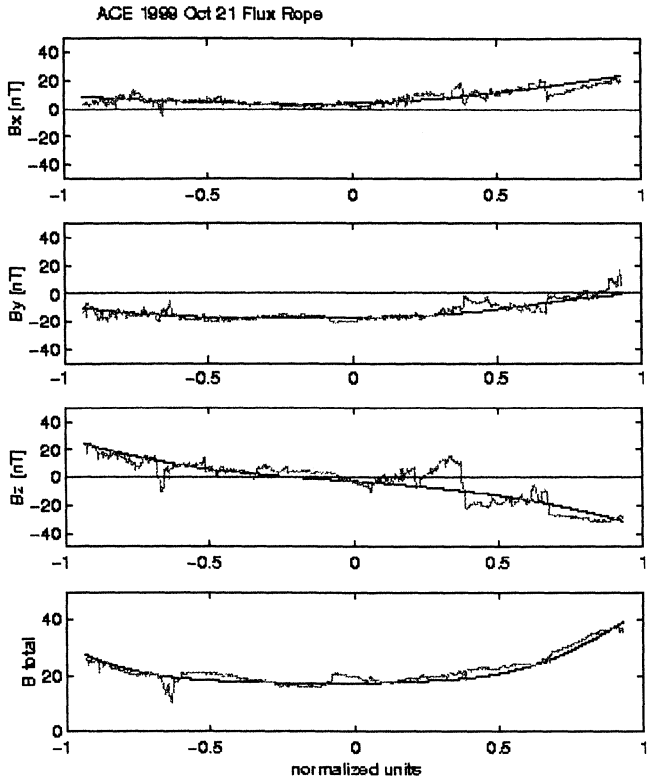

Figure 14. The magnetic field components of the flux rope model overlapped on the ACE magnetic field data between the two vertical dashed lines in Figure 10 for the October 21, 1999 ICME, where the smooth dark lines are the model and the lighter lines are Wind magnetic field data.

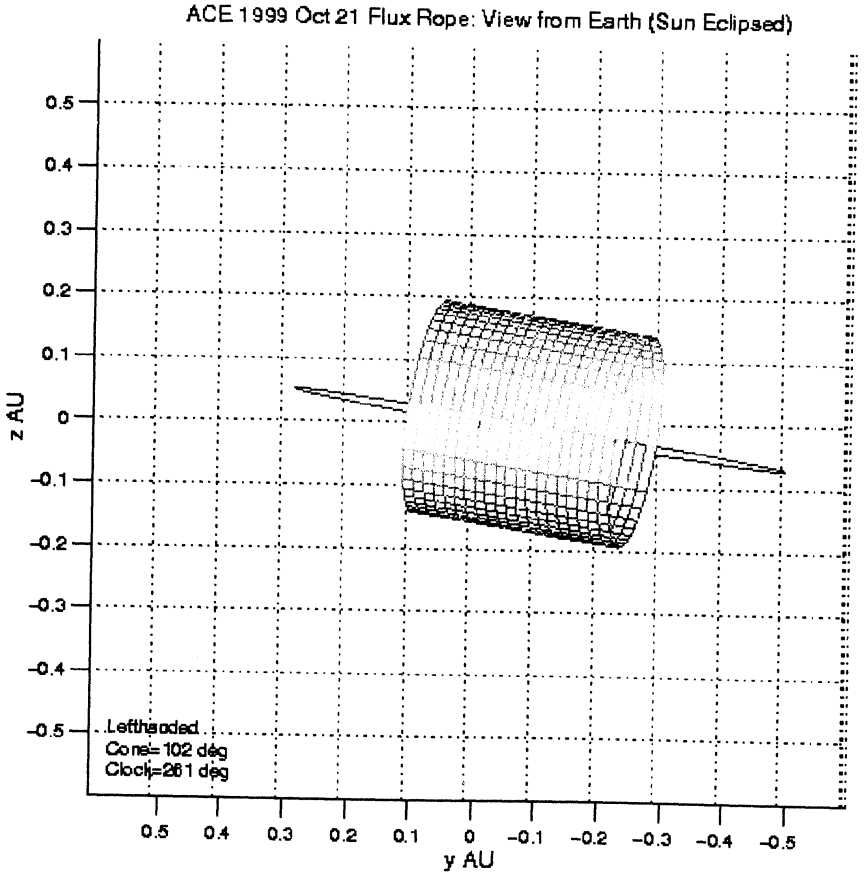

Figure 15. A 3-D cylinder of the modeled flux rope for the October 21, 1999 ICME, viewed from the Earth. The orientation does not agree with the newly opening field arcade in Figure 3a.

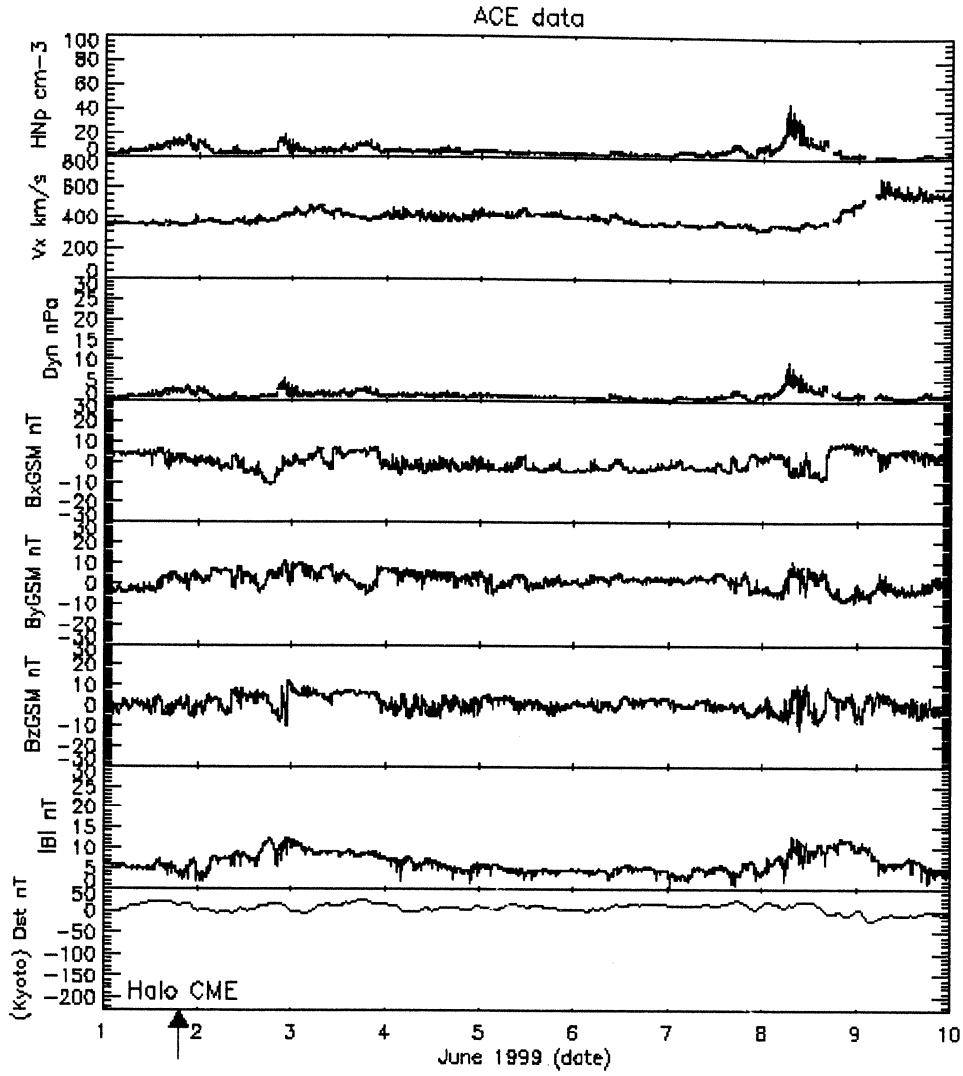

Figure 16. Same as in Figure 10, but for June 1 to 9, 1999, from ACE.

June 26 merely 34 hours after the halo CME are considered not associated with this CME because of the short time delay. The solar wind speed was ~ 380 km/s at the time of the disturbances, and Wind spacecraft observed the same speed during the disturbances and ~ 350 km/s just before the disturbances when ACE had a large data gap. The signatures at the end of June 27 and beginning of June 28, with a density spike, a speed increase, and short magnetic disturbances, may possibly be associated with the CME; however, these cannot be the major part of the ICME (see further discussion in section 6).

6. Related Geomagnetic Storm Activities

The occurrence of geomagnetic storms is typically inferred from the *Dst* index produced by World Data Center C2 (WDC2) at Kyoto (available at http://swdcdb.kugi.kyoto-u.ac.jp/dstdir/ (1998, 1999)). The solar wind data figures presented in section 5 include Kyoto *Dst* for the same time periods including and following the halo CMEs observed by LASCO.

Recall that on January 6, 1997, when LASCO reported a halo CME (example 1; section 3.1); we found newly opening field lines near disk center (see Figure 1) and an ICME in the Wind data ~82 hours later. The *Dst* plot in the bottom panel of Figure 7 shows a geomagnetic storm starting at about the same time when the associated B_z was turning south, reaching a minimum of -96 nT midday on January 10, and begins to decay gradually when the B_z turns north. Again, on October 15, 1998, when LASCO reported a halo CME (example 2; section 3.2), we found newly opening field lines near the disk center (see Figure 2) and an ICME in the ACE solar wind data ~84 hours later. In the *Dst* plot at the bottom of Figure 10 a geomagnetic storm starts at about the time when the ICME-related B_z was turning south, reaching a minimum of -112 nT midday on October 19, and similar to the previous case begins to decay when the B_z turns north. Following the October 18, 1999, LASCO halo CME (example 3;

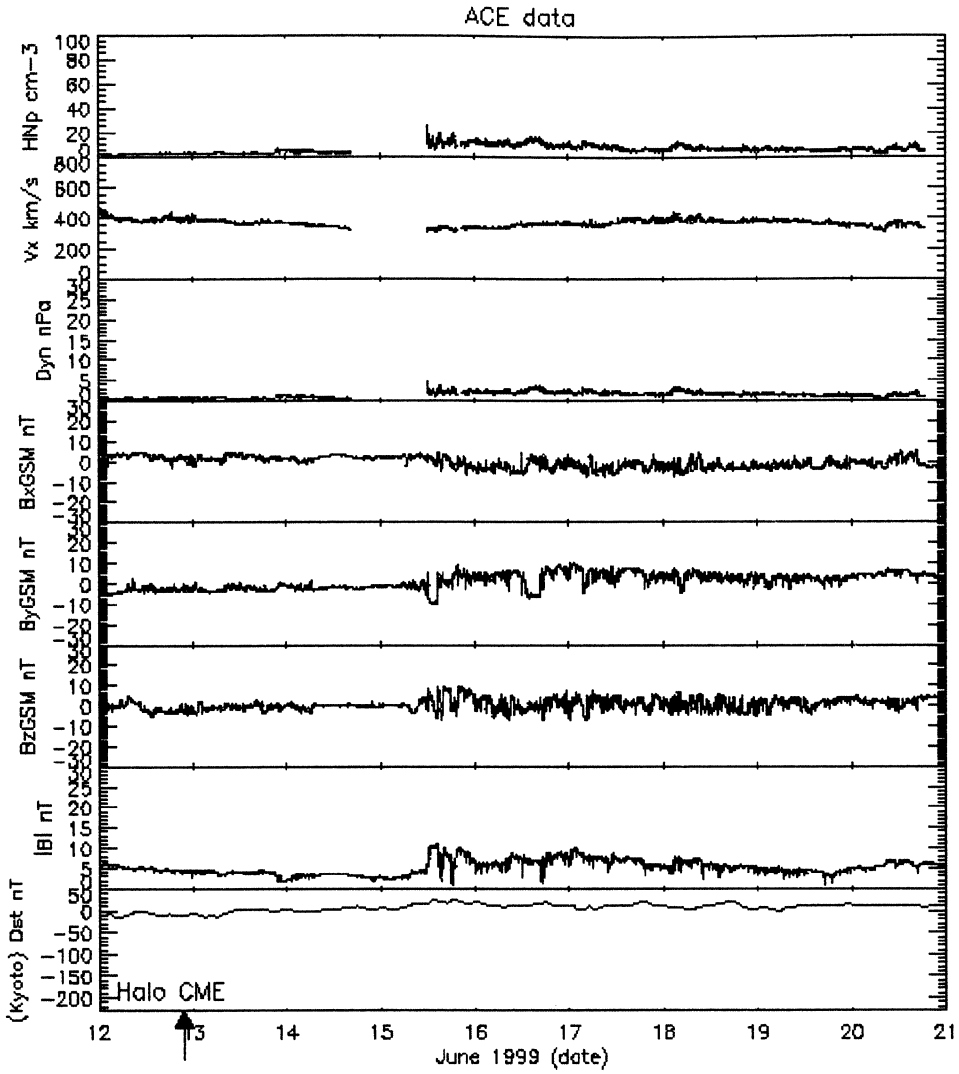

Figure 17. Same as in Figure 10, but for June 12 to 20, 1999, from ACE.

section 3.3), again we found newly opening field lines near disk center (see Figure 3), followed by some relatively complex interplanetary signatures in the ACE solar wind data 72 hours later, including a long lasting strong southward B_z. A large geomagnetic storm began when the ICME related B_z was turning south, reaching a minimum of -231 nT, as seen in the bottom panel of Figure 13.

In contrast, on June 1, 1999, when LASCO reported a bright halo CME (example 4; section 3.4), we found few newly opening field lines near disk center (see Figure 4). This halo event was followed by the quiet solar wind conditions seen in Figure 16. In the bottom panel of Figure 16, correspondingly quiet geomagnetic conditions persist, with *Dst* around zero level for all the next several days shown in the plot. Similarly, on June 12 when LASCO reported a halo CME (example 5; section 3.5), we found no newly opening field lines near disk center (see Figure 5), followed by quiet solar wind conditions and no geomagnetic storm evident in the *Dst* index as see in Figure 17. Finally, for the LASCO halo event on June 24 (example 6; section 3.6), we again found no newly opening field lines near disk center (see Figure 6). In the bottom panel of Figure 18 some small excursions in the *Dst* index are clearly associated with the weak disturbances in the solar wind. While we have noted earlier that these disturbances started too soon to be related to the reported halo CME, the feature at the end of the disturbed period, with a high speed, high density spike, and rotating magnetic fields, is curious. It arrived ~80 hours after the CME, which is not consistent with the apparent high speed of over 800 km/s seen in the solar wind at 1 AU, but the CME speed does not have to be constant during its journey to 1 AU [e.g., *Lindsay et al.*, 1999]. In any case, the short duration of the feature suggests it may be the edge of an ICME that was not centrally directed toward the Earth.

7. Discussion and Conclusion

Among the six reported halo/partial halo CMEs studied, three of them with newly opening field lines near disk center were followed by ICMEs in the Wind or ACE data and geomagnetic storms in the Kyoto *Dst* records

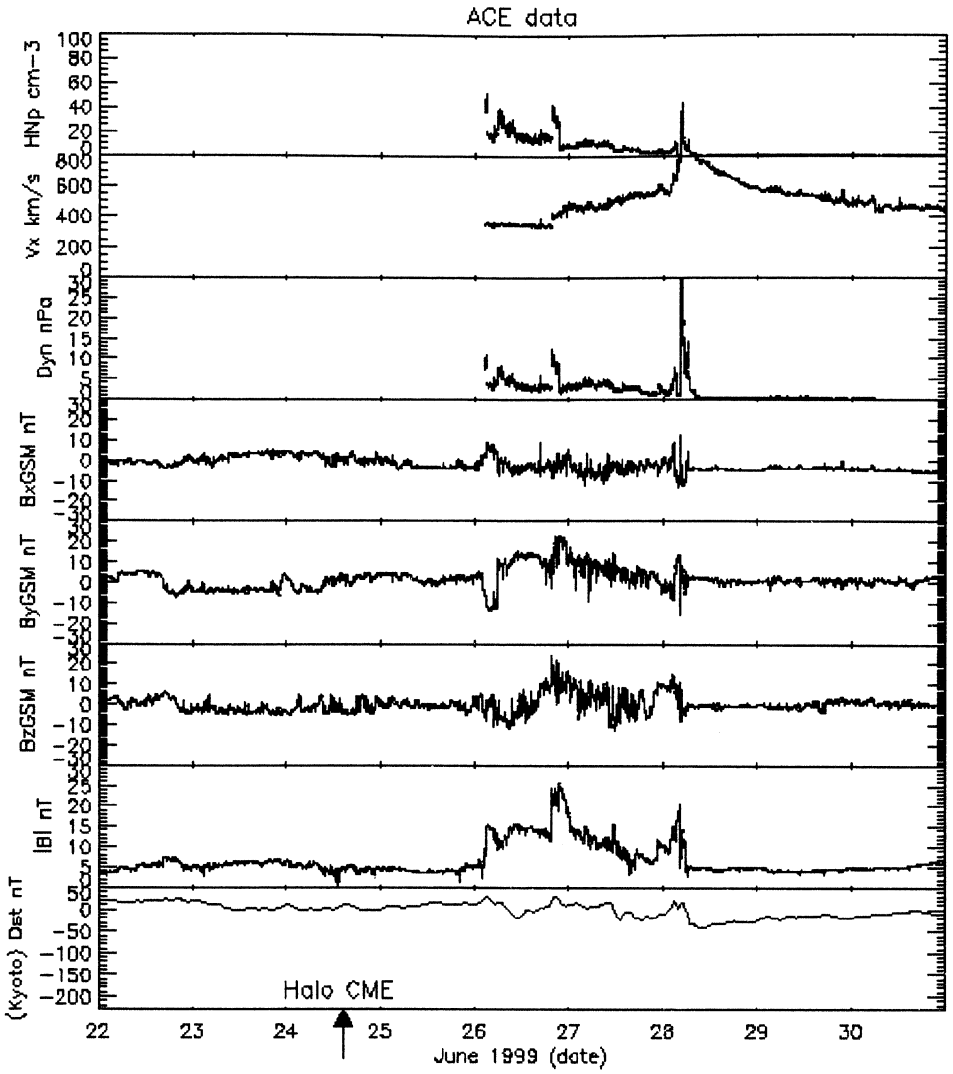

Figure 18. Same as in Figure 10, but for June 22 to 30, 1999, from ACE.

within a few days. The other three with no newly opening field lines near disk center were followed by quiet solar wind and geomagnetic conditions. While these samples do not represent the general LASCO halo event data set, one can find many halo CMEs that are not followed by geomagnetic storms, especially in the recent years of increasing solar activity (1998 - 2000). *Webb et al.* [1999] found that among seven frontside halo CMEs just after solar minimum, six had geomagnetic storms ranging from Dst = -33 to - 115. Near solar maximum it is more difficult to conduct such a study, and the results may not be the same, as suggested by the examples of this study. *St. Cyr et al.* [2000] reported the properties of all 841 CMEs observed by SOHO/LASCO from January 1996 through June 1998, among which 92 are halo or partial halo CMEs. They then used full disk SOHO/EIT images to eliminate backside halo CMEs and found 40 frontside halo CMEs. The comparison between the frontside halo CMEs and the Kp geomagnetic storm index showed that the "false alarm" rate was high, but 15 out of 18 of the $Kp \geq 6$ storms (when SOHO has observations) could be accounted for as frontside halo CMEs. The results demonstrated the importance for discriminating geoeffective CMEs with further criteria.

LASCO observations are the most direct means of observing potentially geoeffective halo CMEs soon after the events take place near the Sun. However, because of the nature of halo CMEs, there is unavoidable ambiguity from a line of sight observation. It is necessary to rely on other observations, usually EIT waves, EIT and soft X-ray flares, disappearing filaments, soft X-ray sigmoids, and other disk activities, to exclude backside halo CMEs and misleading limb events. The results of this study suggest that like other disk activities, monitoring the coronal large-scale magnetic field behavior can reinforce (or not) predictions of magnetic storms based on LASCO halo CMEs. Moreover, the coronal field over the visible hemisphere contains information about the possible geoeffectiveness of a particular CME because it shows the approximate orientation and location of the active arcades. Among the three cases in

1997, 1998 and 1999, when we fitted flux ropes to ICME magnetic field data, we found agreement between the flux rope orientation and the newly opening field arcade orientation for two events in 1997 and 1998.

We recognize that potential field source surface models are limited, especially in applications to the active corona [e.g., see *Mikic and Linker*, 1994]. Our goal is to ultimately see this procedure for inferring coronal field activity applied to a more realistic model such as the 3-D MHD global simulations of *Linker et al.* [1999] with photospheric vector field boundary conditions. We also need to determine the importance of the timescale for the synoptic map updates given that the important changes may occur on smaller time-scales than a day, especially around solar maximum. Observations from the Global Oscillation Network Group network of ground-based magnetographs and SOHO/Michaelson Doppler Imager are currently under study with this goal in mind. It should also be noted that this procedure is only as good as the assumption that the global coronal magnetic field, and the changes therein, can be reconstructed by looking at the photospheric field on the visible disk alone. Clearly, a heliocentric constellation of magnetographs would be most desirable for future applications of this concept to space weather predictions by coronal magnetic field monitoring.

Acknowledgments. The work at UCB was supported by NASA SEC-GI Program NAG5-7951 and NSF Space Weather Program 98-19776. The work at UCLA was in part supported by a grant from IGPP/LANL. O.C.S. wishes to acknowledge partial support by NASA contract S-86760-E and by the National Space Weather Program under NSF grant ATM-9819668. The ACE data used here are provided to the community via the ACE Science Center at Caltech. We thank the ACE Science Center personnel as well as the instrument PIs D.J. McComas and C.W. Smith for making the ACE plasma and magnetic field data available and K. W. Ogilvie and R. P. Lepping for the Wind plasma data and magnetic field data archive resource.

Hiroshi Matsumoto thanks J. R. Burkepile and another referee for their assistance in evaluating this paper.

References

Altschuler, M. D., and G. Newkirk, Jr., Magnetic fields and the structure of the solar corona I, *Sol. Phys.*, *9*, 131, 1969.

Altschuler, M. D., R. H. Levine, M. Stix, and J. Harvey, High resolution mapping of the magnetic field of the solar corona, *Sol. Phys.*, *51*, 345, 1977.

Arge, C. N., and V. J. Pizzo, Improvement in the prediction of solar wind conditions using near-real time solar magnetic field updates, *J. Geophys. Res.*, *105*, 10465, 2000.

Brueckner, G. E, et al., The Large Angle Spectroscopic Coronagraph (LASCO), *Sol. Phys.*, *162*, 357, 1995.

Burlaga, L. F., Magnetic clouds and force-free fields with constant alpha, *J. Geophys. Res.*, *93*, 7217, 1988.

Canfield, R. C., H. S. Hudson, and D. E. McKenzie, Sigmoidal morphology and eruptive solar activity, *Geophys. Res. Lett.*, *26*, 627, 1999.

Gibson, S. E., et al., The three-dimensional coronal magnetic field during Whole Sun Month, *Astrophys. J.*, *520*, 871, 1999.

Gosling, J. T., Coronal mass ejections and magnetic flux ropes in interplanetary space, in *Physics of Magnetic Flux Ropes, Geophys. Monog. Ser.*, vol. 58, edited by C. T. Russell, E. R. Priest, and L. C. Lee, p. 343, AGU, Washington, D. C., 1990.

Gosling, J. T., E. Hildner, R. M. MacQueen, R. H. Munro, A. I. Poland, and C. L. Ross, Mass ejections from the Sun: A view from Sklyab, *J. Geophys. Res.*, *79*, 4581, 1974.

Gosling, J. T., D. J. McComas, D. J., J. L. Phillips, and S. J. Bame, Geomagnetic activity associated with Earth passage of interplanetary shock disturbances and coronal mass ejections, *J. Geophys. Res.*, *96*, 7831, 1991.

Hoeksema, J. T., Structure and evolution of the large scale solar and heliospheric magnetic fields, Ph.D. thesis, Stanford Univ., Stanford, Calif., 1984.

Hoeksema, J. T., The large-scale structure of the heliospheric current sheet during the Ulysses epoch, *Space Sci. Rev.*, *72*, 137, 1995.

Lepping, R. P., J. A. Jones, and L. F. Burlaga, Magnetic field structure of interplanetary magnetic clouds at 1 AU, *J. Geophys. Res.*, *95*, 11,957, 1990.

Lepping, R. P., et al., The Wind magnetic field investigation, *Space Sci. Rev.*, *71*, 207, 1995.

Levine, R. H., Open magnetic fields and the solar cycle I, *Sol. Phys.*, *79*, 203, 1982.

Levine, R. H.; M. Schulz, and E. N. Frazier, Simulation of the magnetic structure of the inner heliosphere by means of a non-spherical source surface, *Sol. Phys.*, *77*, 363, 1982.

Li, Y., J. G. Luhmann, J. T. Hoeksema, X. P. Zhao, and C. N. Arge, Visualizing CMEs and predicting geomagnetic storms from solar magnetic fields, in *Space Weather, Geophys. Monog. Ser.*, vol. 124, edited by P. Song, H. Singer, and G. Siscoe, pp. 167, AGU, 2001.

Lindsay, G. M., J. G. Luhmann, C. T. Russell, and J. T. Gosling, Relationships between coronal mass ejection speeds from coronagraph images and interplanetary characteristics of associated interplanetary coronal mass ejections, *J. Geophys. Res.*, *104*, 12,515, 1999.

Linker, J. A. and Z. Mikic, Disruption of a helmet streamer by photospheric shear, *Astrophys. J.*, *438*(1), L45, 1995.

Linker, J. A., Z. Mikic, D. A. Biesecker, R. J. Forsyth, S. E. Gibson, A. J. Lazarus, A. Lecinski, P. Riley, A. Szabo, and B. J. Thompson, Magnetohydrodynamic modeling of the solar corona during Whole Sun Month, *J. Geophys. Res.*, *104*, 9809, 1999.

Luhmann, J. G., J. T. Gosling, J. T. Hoeksema, and X. P. Zhao, The relationship between large-scale solar magnetic field evolution and coronal mass ejections, *J. Geophys. Res.*, *103*, 6585, 1998.

McAllister, H., and S. F. Martin, The essential role of magnetic reconnection in erupting prominences and CMEs, , *Adv. Space Res.*, *26*,(3), 469, 2000.

McComas, D. J., J. T. Gosling, C. M. Hammond, M. B. Moldwin, J. L. Phillips, and R. J. Forsyth, Reconnection on open field lines ahead of CMEs, *Space Sci. Rev.*, *72*, 129, 1995.

McComas, D.J., S.J. Blame, P. Barker, W.C. Feldman, J.L. Phillips, P. Riley, and J.W. Griffee, Solar Wind Electron Proton Alpha Monitor (SWEPAM) for the Advanced Composition Explorer, *Space Sci. Rev.*, *86*, 561, 1998.

Mikic, Z., and J. A. Linker, Disruption of coronal magnetic field arcades, *Astrophys. J.*, *430*(2), 898, 1994.

Mulligan, T., and C. T. Russell, Multi-spacecraft modeling of the flux rope structure of interplanetary coronal mass ejections: Cylindrically symmetric versus non-symmetric topologies, *J. Geophys. Res.*, in press, 2001.

Mulligan, T., C. T. Russell, and J. G. Luhmann, Solar cycle evolution of the structure of magnetic clouds in the inner heliosphere, *Geophys. Res. Lett.*, *25*, 2959, 1998.

Munro, R. H., J. T. Gosling, E. Hildner, R. M. MacQueen, A. I. Poland, and C. L. Ross, The association of coronal mass ejection transients with other forms of solar activity, *Sol. Phys., 61,* 201, 1979.

Odstrcil, D., and V. J. Pizzo, Three-dimensional propagation of CMEs in a structured solar wind flow, 1, CME launched within the streamer belt, *J. Geophys. Res., 104,* 483, 1999.

Ogilvie, K.W., et al., A comprehensive plasma instrument for the Wind spacecraft, *Space Sci. Rev., 71,* 55, 1995.

Plunkett, S. P., B. J. Thompson, R. A. Howard, D. J. Michels, O. C. St. Cyr, S. J. Tappin, R. Schwenn, and P. L. Lamy, LASCO observations of an Earth-directed coronal mass ejection on May 12, 1997, *Geophys. Res. Lett., 25,* 2477, 1998.

Schatten, K. H., J. M. Wilcox, and N. F. Ness, A model of interplanetary and coronal magnetic fields, *Sol. Phys., 6,* 442, 1969.

Smith, C.W., M.H. Acuna, L.F. Burlaga, J. L'Heureux, N.F. Ness, and J. Scheifele, The ACE Magenetic Fields Experiment, *Space Sci. Rev., 86,* 611, 1998.

St. Cyr, O. C., et al., Properties of coronal mass ejections: SOHO/LASCO observations from January 1996 to June 1998, *J. Geophys. Res., 105,* 18,169, 2000.

Thompson, B. J., S. P. Plunkett, J. B. Gurman, J. S. Newmark, O. C. St. Gyr, and D. J. Michels, SOHO, EIT observations of an Earth-directed coronal mass ejection on May 12, 1997, *Geophys. Res. Lett., 25,* 2465, 1998.

Wang, Y.-M., N. R. Sheeley, Jr., On potential field models of the solar corona, *Astrophys. J., 392,* 310, 1992.

Webb, D. F., E. W. Cliver, N. Gopalswamy, H. S. Hudson, and O. C. St. Cyr, The solar origin of the January 1997 coronal mass ejection, magnetic cloud, and geomagnetic storm, *Geophys. Res. Lett., 25,* 2469, 1998.

Webb, D. F., E. W. Cliver, E. W., N. U. Crooker, O. C. St. Cry, and B. J. Thompson, Relationship of halo coronal mass ejections, magnetic clouds, and magnetic storms, *J. Geophys. Res., 105,* 7491, 2000.

Zhao, X. P., and J. T. Hoeksema, Effect of coronal mass ejections on the structure of the heliospheric current sheet, *J. Geophys. Res., 101,* 4825, 1996.

Zhao, X. P., J. T. Hoeksema, and P. H. Scherrer, Changes of the boot shaped coronal hole boundary during Whole Sun Month near sunspot minimum, *J. Geophys. Res., 104,* 9735, 1999.

C. N. Arge, NOAA, Space Environment Center, 325 Broadway, MS: R/E/SE, Boulder, Colorado, USA 80303. (nick.arge@noaa.gov)

J. T. Hoeksema, Stanford Univ., H.E.P.L. Annex B213, Stanford, CA 94305-4085, USA. (todd@quake.stanford.edu)

Y. Li and J. G. Luhmann, Space Sciences Laboratory, University of California, Berkeley, CA 94720, USA. (yanli@ssl.berkeley.edu; jgluhman@ssl.berkeley.edu)

T. Mulligan, Institute of Geophysics and Planetary Physics and the Department of Earth and Space Sciences, University of California, Los Angeles, CA 90096-1567, USA. (tamitha@igpp.ucla.edu)

S. P. Plunkett, USRA, Mail Code 682.3, Naval Reasearch Laboratory, Greenbelt, MD 20771, USA. (plunkett@ajcannon.nascom.nasa.gov)

O. C. St. Cyr, Computational Physics, Inc. and The Catholic University of America, NASA-Goddard Space Flight Center, USA. (stcyr@cua.edu)

(Received November 27, 2000; revised March 26, 2001; accepted March 26, 2001.)